Russian Journal of Earth Sciences Online ISSN: 1681-1208

Special Issue: "Kamchatka Earthquake M 8.8 on July 29, 2025"

Crustal Movements and Deformations in Relation to Seismicity in Continuation of the Preparation Period of the Kamchatka Megathrust Earthquake (2020–2025)

P. A. Dokukin[1], V. I. Kaftan[*,2], N. N. Titkov[3], and D. V. Chebrov[3]

[1] RUDN University, Moscow, Russian Federation
[2] Geophysical Center of RAS, Moscow, Russian Federation
[3] Kamchatka Branch of the Geophysical Survey of the Russian Academy of Sciences, Petropavlovsk-Kamchatsky, Russian Federation
* **Correspondence to:** Vladimir Kaftan, v.kaftan@gcras.ru

Abstract: This study presents the results of a spatiotemporal analysis of crustal movements and deformations obtained by processing regional GNSS network data for a five-year period prior to the 2025 Kamchatka megaquake. The control network consisted of twenty-two continuously operating GNSS stations. Station spacing varied from 100 to 2500 km. An assessment was made of the sparse regional network's response capabilities to the preparation of one of the strongest seismic events in history. Kinematic models were obtained for the evolution of internal displacement deficits, horizontal shear strains, and dilatation. The area of accumulated displacement deficit is regularly distributed along the Kuril–Kamchatka Trench, demonstrating resistance to the unidirectional northwestward translational motion of the Pacific tectonic plate. The evolution of total shear strain is consistent with the hypothesis of a possible triggering effect on the mature seismic source of the Kamchatka megathrust. The spatial distribution of accumulated dilatational strain reflects regional tectonic features previously identified by geophysical and geological studies. The results demonstrate the effectiveness of using sparse continuous GNSS observation networks to assess general regional geodynamic and tectonic trends in preparation of the 2025 Kamchatka megathrust.

Keywords: GNSS, internal displacement deficit, crustal movements, crustal deformations, earthquake forecast, Kamchatka megathrust earthquake

Citation: Dokukin P. A., Kaftan V. I., Titkov N. N., and Chebrov D. V. (2026), Crustal Movements and Deformations in Relation to Seismicity in Continuation of the Preparation Period of the Kamchatka Megathrust Earthquake (2020–2025) , *Russian Journal of Earth Sciences*, 26, ES2007, EDN: SRYHRR, https://doi.org/10.2205/2026es001117

Research Article

Received: February 2, 2026
Accepted: May 25, 2026
Published: July 1, 2026

1. Introduction

A recent powerful earthquake off the coast of Kamchatka has sparked significant interest among researchers in studying the processes directly related to its occurrence. This rare event ranks among the top ten most powerful historical earthquakes, holding the sixth position in terms of magnitude, and has been the strongest in the region since 1952. One unexpected circumstance, however, was the complete absence of human fatalities and the minimal level of damage to buildings and structures. Its epicenter was located about one hundred and fifty kilometers from Petropavlovsk-Kamchatsky, with the source occupying an area of approximately 400×150 km [*Chebrov*, 2025]. The earthquake generated a significant tsunami, the maximum impact of which was felt on the uninhabited part of the southern Kamchatka coast [*Pinegina et al.*, 2026]. However, the port of Severo-Kurilsk was damaged, though human fatalities were avoided.

Moreover, it is important to note that such a minimal level of destruction and the absence of fatalities were ensured thanks to the efforts of Russian scientists, among whom Academician Sergey Alexandrovich Fedotov holds a special place. He is not only the author of long-term forecasts of the region's seismic activity [*Fedotov and Solomatin*, 2019] but also the principal initiator of engineering measures to strengthen and provide seismic protection for buildings and structures in Petropavlovsk-Kamchatsky.

The study of crustal movements and deformations in seismically active regions plays a significant role in researching the preparation phases of strong earthquakes. The authors of this publication have years of experience in such studies based on data from continuous GNSS observations. The 2025 Kamchatka megathrust earthquake has sparked interest in the spatiotemporal analysis of crustal movements and deformations over the five-year period preceding the event. Given the high magnitude of the earthquake, we analyzed data from the GNSS observation network covering a fairly large region. For various reasons, the density of GNSS stations in this network is low. Nevertheless, it is not advisable to ignore the observation data from these stations. Furthermore, this very fact motivated the authors to conduct research, including an assessment of the network's capability to detect the preparation of one of the most powerful seismic events in history.

2. Regional Tectonics and the Strongest Earthquakes

The main tectonic structures of the region are the Kuril–Kamchatka and Aleutian island arcs. They were formed under the influence of the interaction between the Pacific and Eurasian global tectonic plates. This is carried out indirectly through the supposed Kamchatka and Okhotsk blocks. The North American global tectonic plate adjoins the region from the north.

The most important tectonic elements of the area affected by the Kamchatka megathrust earthquake (July 29, 2025, $M = 8.8$) are the Kuril–Kamchatka and Aleutian deep-sea trenches. They were formed by the process of oceanic crust subducting beneath the continental tectonic plate. Typical structures include forearc basins accompanied by uplifts, and deep-water back-arc basins on the periphery of the island arc complexes.

Here, the Aleutian tectonic dislocations have a right-lateral strike-slip mechanism, while the Kuril–Kamchatka branch experiences thrust displacements. The Aleutian fault system continues onto the Cape Kamchatsky Peninsula, where high rates of crustal uplift have been recorded. The tectonic model of this zone is presented in this paper [*Gaedicke et al.*, 2000].

Of significant interest in the context of this rare and large-scale seismic event are such marine structural formations [*Pushcharovsky*, 2011] as the Emperor Rise and the Shirshov Ridge. These ridges act as tectonic boundaries between the morphostructural sectors of the Pacific Ocean and the Bering Sea. They host numerous submarine volcanoes and are experiencing uplift on geological timescales.

The Emperor Rise is represented by an elongated, sub-meridionally oriented chain of submarine ridges (guyots), stretching from the Hawaiian Islands to the junction of the Kuril–Kamchatka and Aleutian deep-sea trenches. The formation of the Emperor Rise is explained by the movement of the Pacific Plate over a stationary hot spot (mantle plume), currently located in the Hawaiian Islands region.

Nevertheless, this hypothesis faces objections, for example, from A. A. Peive, who believed that the primary role in the formation of such oceanic rises lies in deep-seated faulting and lateral mantle flows with shear displacements [*Pushcharovsky*, 2011]. An interesting geotectonic object in the area of the northern termination of the Emperor Rise is a magmatic plume [*Gorbatov et al.*, 2001]. The authors studied earthquake catalogs from 1955–1998, obtained from the Geophysical Service of Russia, the International Seismological Centre, and the National Earthquake Information Center of the US Geological Survey. Seismic tomography results showed that a low-velocity anomaly beneath Meiji Guyot originates at a depth of about 1000 km and continues upward to depths of less than 200 km. In its upper part, it begins to extend sub-horizontally in the direction of

Table 1. The Strongest Historical Earthquakes in the Kuril–Kamchatka Region from 1900 to 2025 ($M > 8$)

No.	Date	Geographic position	Lat.	Long.	M	Depth
1	1918-11-08	Kuril Islands	44.998	152.320	8.1	15.0
2	1923-02-03	Kamchatka Gulf	54.486	160.472	8.4	15.0
3	1952-11-04	Southern Kamchatka	52.623	159.779	9.0	21.6
4	1958-11-06	Kurilsk	44.479	148.485	8.3	35.0
5	1994-10-04	Shikotan	43.773	147.321	8.3	14.0
6	2006-11-15	Kuril Islands	46.592	153.266	8.3	10.0
7	2007-01-13	Kuril Islands	46.243	154.524	8.1	10.0
8	2013-05-24	Sea of Okhotsk	54.892	153.221	8.3	598.1
9	2025-07-29	Kamchatka Peninsula	52.495	160.240	8.8	35.0

the Pacific Plate's motion. The territorial proximity of this object to the epicentral zone of the Kamchatka megathrust earthquake necessitates taking it into account in geodynamic analysis.

According to the plate tectonic model, the primary source of tectonic stress in the region is the northwestward movement of the Pacific Plate at an average speed of about 7.5 cm/year. Meanwhile, in the southern part of the region, this plate movement is estimated to be at a higher rate of 8.2 cm/year [*Avdeiko et al.*, 2007; *Steblov et al.*, 2010].

From 1900 to 2025, nine earthquakes with a magnitude greater than 8.0 occurred in the Kuril–Kamchatka region. The events are presented in Table 1 based on archive data https://earthquake.usgs.gov/earthquakes/browse/significant.php

The strongest earthquakes occurred near the Kamchatka Peninsula with a recurrence interval of 73 years and a distance of 32 kilometers between their epicenters.

3. Observation Network, Initial Data and Processing

For the analysis of the spatiotemporal evolution of recent crustal movements and deformations in the region, a network of 22 continuous GNSS stations was formed. Coordinate solutions for stations located on the Kamchatka Peninsula and the nearest islands, which are part of the regional KAMNET network, were provided by researchers from the Kamchatka Branch of the Unified Geophysical Service of the Russian Academy of Sciences.

Coordinate time series for the remaining stations in Russia, Japan, and the USA were obtained from the web-archive of the Nevada Geodetic Laboratory (Reno, USA) [*Blewitt et al.*, 2018]. The duration of the time series for each coordinate (East, North, Up) was 2027 values for each GNSS station.

The coordinate time series for the KAMNET network were derived by processing dual-frequency GNSS phase measurements using the double-differenced GPS carrier phase method, with reference to 190 stations of the IGS network. The processing by the Nevada Geodetic Laboratory was performed using the Precise Point Positioning (PPP) method. In both cases, the final products of the International GNSS Service (IGS) were utilized. The coordinates of all stations were determined in the ITRF2020 reference frame with sub-centimeter accuracy. A map of the established GNSS network is presented in Figure 1.

It can be seen that the control network covers an extensive region, a large part of which is a marine area. Consequently, the GNSS stations are relatively sparsely distributed. The mutual distances of GNSS stations from each other in the formed control network are generally in the order of several hundreds of kilometers. Given that the seismic source of the megathrust earthquake extends several hundred kilometers and coseismic crustal displacements can propagate for thousands of kilometers, it was decided to use this selected, non-dense network for a general assessment of crustal movements and deformations over a long time interval.

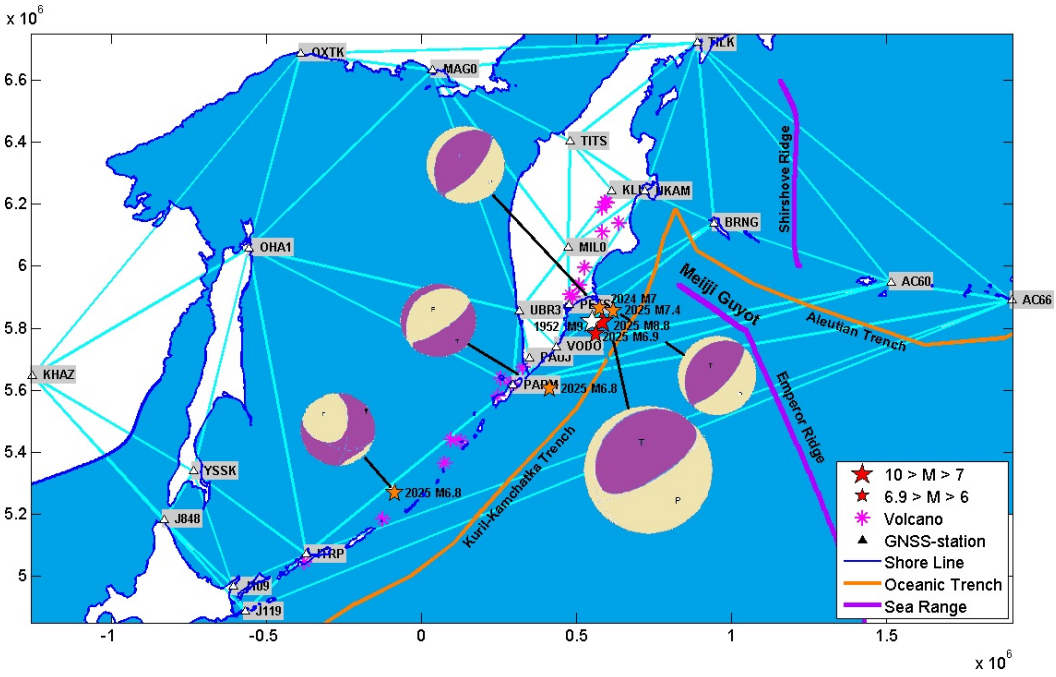

Figure 1. Map of the study region. Observation network, principal tectonic elements, and the strongest earthquakes of 2024–2025. To the right of the GNSS station triangle symbol in all illustrations, its four-character official name is written. The sides of the triangles of the Delaunay triangulation are shown in light blue. The frame values of the cartographic coordinate grid of the UTM projection (zone 57N) at all figures are given in meters. Red stars – the 2025 megathrust earthquake and its strong aftershock. Orange stars – strong earthquakes preceding the megathrust earthquake. White star – the 1952 megathrust earthquake. Focal mechanisms are sourced from https://earthquake.usgs.gov/earthquakes/browse/significant.php.

The initial epoch for the coordinate time series was set to 2020-01-01, and the final epoch to 2025-08-01. Gaps in the observation continuity were eliminated by interpolating coordinates for the missing dates using Hermit splines.

To correlate crustal movements and deformations with the progression of the seismic process, an earthquake catalog obtained from the National Earthquake Information Center (NEIC) was used. https://earthquake.usgs.gov/earthquakes/search/. A total of 1,653 seismic events with magnitudes greater than 4.5 were selected.

To analyze the contribution of specific strong earthquakes to the geodynamic process, a set of strong earthquakes with $M > 6.5$, presented in Table 2, was utilized.

The geographical positions of volcanoes in the region that have been active in historical times were obtained from the online resource https://volcano.si.edu/reports_bgvn.cfm (based on data from the Global Volcanism Program, Smithsonian Institution, USA).

Let us consider the equation of motion for a system of material points within the framework of classical mechanics

$$\Sigma \overline{F}_i = \overline{F}_0 + \Sigma \overline{f}_i, \tag{1}$$

where $\overline{F}_0$ – the resultant of external forces, $\overline{f}_i$ – internal forces, i – the running index of a material point.

Expanding the expressions for the forces, Equation (1) can be written as:

$$\Sigma \overline{a}_i m_i = \overline{a}_0 \Sigma m_i + \Sigma \overline{a}'_i m_i, \tag{2}$$

where $\overline{a}_i$ – total accelerations, $\overline{a}'_i$ – internal accelerations, $\overline{a}_0$ – resultant external acceleration, m_i – masses of material points.

Table 2. Strong Earthquakes in the Study Region for 2021–2025

No.	Date and Time	Geographic coordinates (°)		Coordinates in UTM57 projection (m)		Depth (km)	Magnitude
		Latitude	Longitude	East	North		
1	2025-07-29 23:24:52.625	52.5116	160.3244	589878	5818766	35	8.8
2	2020-03-25 02:49:21.160	48.9638	157.6955	404517	5424251	57.8	7.5
3	2025-07-20 06:49:04.495	52.8271	160.7907	620648	5854539	34	7.4
4	2024-08-17 19:10:26.820	52.9308	160.1331	576162	5865173	29	7
5	2020-02-13 10:33:44.406	45.6161	148.959	−282758	5100664	143	7
6	2025-07-30 00:09:57.929	52.1605	159.9138	562507	5779283	25.3	6.9
7	2025-08-03 05:37:55.562	50.5804	157.7988	414955	5603854	35	6.8
8	2024-12-27 12:47:37.696	47.2996	151.236	−86808	5267763	146	6.8
9	2025-07-20 07:23:00.264	52.8703	160.7934	620710	5859349	22.1	6.6
10	2025-07-20 07:07:42.573	52.6981	160.8332	623877	5840264	10	6.6
11	2025-07-20 06:28:17.860	52.9286	160.6233	609115	5865561	23	6.6
12	2021-03-16 18:38:21.233	54.7368	163.1803	769075	6073524	13.2	6.6
13	2024-08-10 03:28:32.681	47.223	144.7915	−574759	5328738	402	6.5
14	2023-12-28 09:15:16.131	44.596	149.0388	−290637	4986574	31	6.5
15	2023-04-03 03:06:57.235	52.7227	158.4935	465791	5841544	101	6.5

Having reduced equal mass sums and time intervals in (2), for the velocity vectors of the movements $\overline{v}_i$ of the displacements $\overline{u}_i$, we obtain the following:

$$\overline{v}_i = \overline{V}_i - \overline{V}_0 \quad \text{and} \quad \overline{u}_i = \overline{U}_i - \overline{U}_0.$$

To identify areas of internal displacement deficit, the magnitudes of the cumulative displacement vectors $|\overline{u}_i|$ from the initial day to the current day were calculated.

For determining deformation characteristics, the horizontal strain tensor was used (with the coordinate axes n and e directed north and east, respectively).

$$T_\varepsilon = \begin{pmatrix} \varepsilon_n & \varepsilon_{ne} \\ \varepsilon_{en} & \varepsilon_e \end{pmatrix}.$$

The tensor components are equal to the partial derivatives of the displacements u_n and u_e with respect to the coordinate axes n and e: $\varepsilon_n = \frac{\partial u_n}{\partial n}$, $\varepsilon_e = \frac{\partial u_e}{\partial e}$, and $\varepsilon_{en} = \varepsilon_{ne} = \frac{1}{2}\left(\frac{\partial u_n}{\partial e} + \frac{\partial u_e}{\partial n}\right)$, respectively, where $\frac{\partial u_n}{\partial e} + \frac{\partial u_e}{\partial n} = \gamma_{ne} = \gamma_{en}$ is the engineering shear strain.

In our study of the spatiotemporal evolution of the seismodeformational process, the following invariant characteristics were used.

1. Principal strains ε_1 and ε_2

$$\varepsilon_{1,2} = \frac{1}{2}\left[\varepsilon_n + \varepsilon_e \pm \sqrt{(\varepsilon_n - \varepsilon_e)^2 + \gamma_{ne}^2}\right].$$

2. Total shear $\gamma = \left((\varepsilon_n - \varepsilon_e)^2 + \gamma_{ne}^2\right)^{1/2}$.
3. Dilatation $\Delta = \varepsilon_1 + \varepsilon_2$.

During the calculation of the strain components, an algorithm was applied [*Wu et al.*, 2006].

The displacement vector modules, dilation and total shear values, as well as vertical displacements, were interpolated onto a regular grid to obtain digital and graphical models of their spatial distribution. For each day, frames of the spatial distribution of deformation characteristics and epicenters of occurring earthquakes were generated, overlaid on maps depicting coastlines, deep-sea trenches, submarine ridges, and active volcanoes.

The resulting frames were compiled into synoptic animations, enabling a heuristic comparative analysis of the behavior of movements and deformations throughout the seismic process.

4. Internal Displacement Deficit and Seismicity

For spatiotemporal analysis of the preparation processes of strong earthquakes, we utilize the value of the internal crustal displacement deficit. This parameter represents the minimal magnitude of the horizontal internal displacement vector at a GNSS station. It is close to the well-known geodetic indicator of seismic hazard – the slip deficit on the surface of a seismogenic fault [*Kocharyan et al.*, 2014; *Materna et al.*, 2023; *Plata-Martinez et al.*, 2024], but not as detailed.

The effectiveness of identifying this parameter depends on the spatial density of the GNSS network stations and the duration of the observation period. The denser the GNSS network and the longer the observations, the higher the accuracy in localizing the zone of elastic strain accumulation.

The evolution of the displacement deficit from 2020 to 2025, with a daily time interval, is tracked in the synoptic animation we created [*Dokukin et al.*, 2025b].

For a comparative analysis of regional seismicity and the behavior of the displacement deficit, the publication presents key frames showing the state immediately before a strong ($M > 6.5$) seismic event and immediately after it (Figures 2–9).

The first two frame pairs of Figure 2 show the absence of visible localized areas of displacement deficit (dark brown zones) in relation to the strong seismic events of February and March 2020. This is explainable by the insufficient time for strain accumulation – approximately four months from the start of observations.

Other contributing circumstances are the significant hypocentral depths of the events, 58 km and 143 km. This indicates a less pronounced surface response to such a deep initiation of seismic source rupture.

At the same time, after nine and a half months, a zone of interaction between the Pacific Plate and the island arcs became clearly visible in the region. The 2 cm isoline, representing the boundary of minor displacements, consistently outlines the Kuril–Kamchatka arc. It is noteworthy that this isoline shifted northwestward following one of the region's deepest earthquakes ($M = 6.4$), which occurred beneath the Earth's crust in the central part of the Kamchatka Peninsula.

It is also interesting that the area of relatively rapid displacements extended northward, encompassing the western segment of the Aleutian Arc.

Observations of the displacement deficit throughout 2021 showed that the area of slow displacements began to narrow, while continuing to consistently follow the alignment of the Kuril Island arc (Figure 3).

The first earthquake of 2021, with $M = 6.6$, occurred east of the Kamchatka Peninsula, 180 km from the coast. Its epicenter coincided with the deep-sea trench line. This event disrupted the configuration of the displacement deficit area, shifting its extreme (the dark brown area) towards the Japanese Archipelago.

The next earthquake, with $M = 6$, was also displaced in the direction of the displacement deficit's migration. It occurred in the area of Onekotan Island without significantly

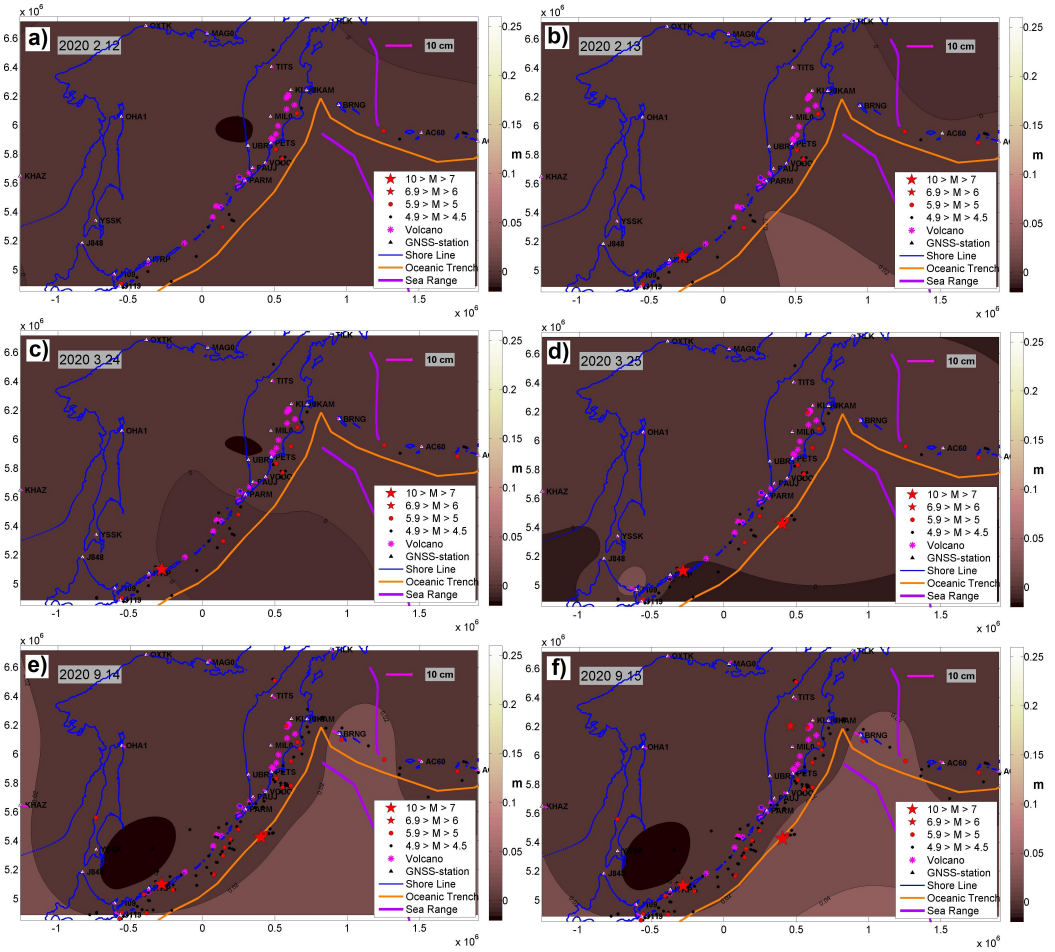

Figure 2. Evolution of the displacement deficit during 2020. a & b – before and after the earthquake of 2020-02-13 (M = 7, Depth = 143 km). c & d – before and after the earthquake of 2020-03-25 (M = 7.5, Depth = 58 km). e & f – before and after the earthquake of 2020-09-15 (M = 6.4, Depth = 344 km). For additional information about the legend, see Figure 1.

altering the zone of slow displacements, which may be explained by the absence of operational GNSS stations in this region.

However, just a month later, the configuration of the displacement deficit anomaly changed substantially, forming a bay-like westward retreat of the zero isoline and an expansion of the area of rapid displacements. This change coincided with the deep earthquake of 2021-09-20 with M = 6.6.

The set of earthquakes in 2021 demonstrated a migration of their epicenters in a southwesterly direction.

Interestingly, the year 2022 is also characterized by three major seismic events, similar to previous observation years, but this time within the Aleutian Arc zone. Two of these, with M = 6.3, occurred in the area of the Aleutian Islands of Alaska (Figure 4a, b, e, f) and had practically no impact on the configuration of the displacement deficit that had formed in the days preceding the events. Their hypocenters were located at relatively great depths of 73–105 km, which may explain the absence of a detectable surface response.

In contrast, the shallow earthquake of 2022-09-20 near Bering Island (Figure 4c, d) with M = 6 broke the general pattern, occurring in an area of relatively rapid displacements near the 10 cm isoline. It is noteworthy that Bering Island demonstrates the highest mobility in the region. Like other GNSS stations in the Aleutian Arc, it is moving northwest due to internal movements, but at a higher rate of 3 cm/year.

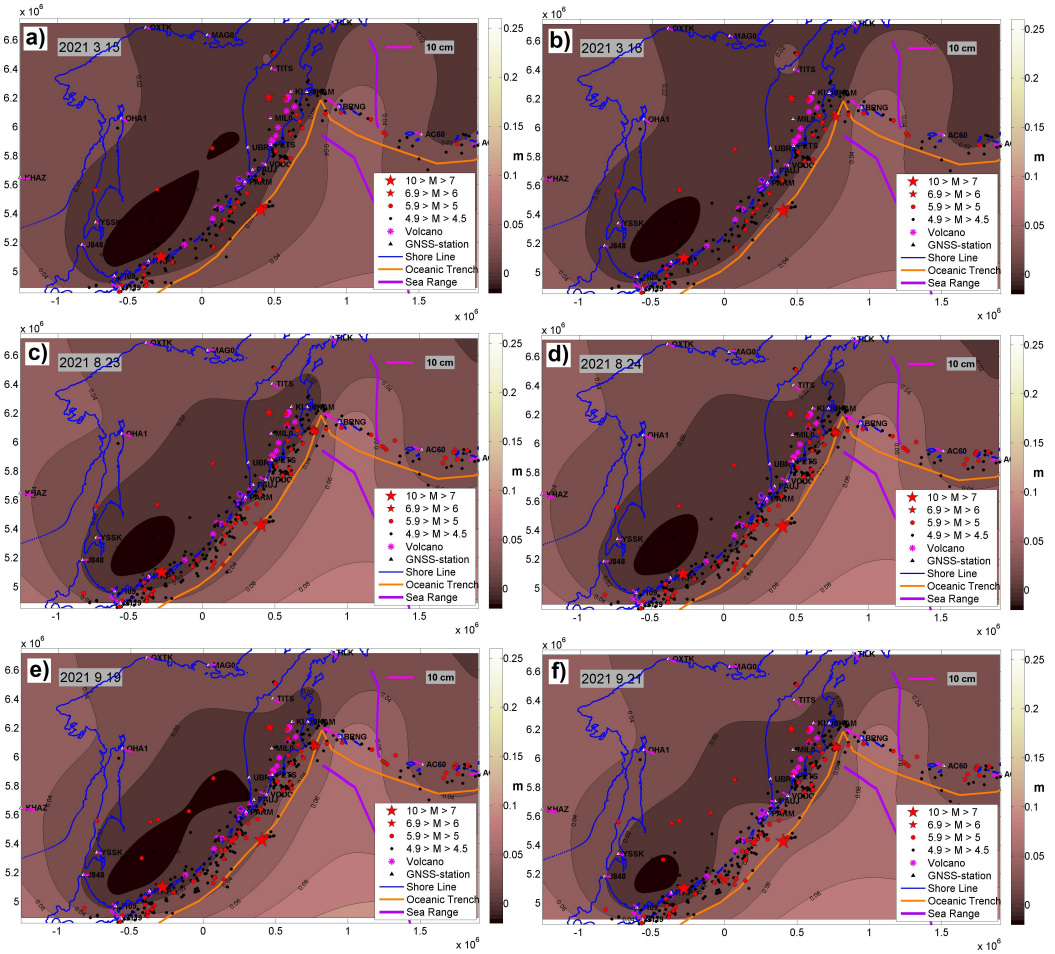

Figure 3. Evolution of the displacement deficit during 2021. a & b – before and after the earthquake of 2021-03-16 (M = 6.6, Depth = 13.2 km). c & d – before and after the earthquake of 2021-08-24 (M = 6, Depth = 35 km). e & f – before and after the earthquake of 2021-09-20 (M = 6.1, Depth = 137 km). For additional information about the legend, see Figure 1.

The greatest interest, however, lies in the synoptic analysis of seismicity and the evolution of the displacement deficit during the period of 2023–2025.

By 2023, the displacement deficit anomaly had formed an elongated area in the back-arc region, with its eastern edge overlapping the elongated zone of earthquake epicenters along the Kuril–Kamchatka arc (Figure 5).

The first major event of the year, with M = 6.5, occurred in Avacha Bay, 60 km south of Petropavlovsk-Kamchatsky, at a relatively great depth (Figure 5a, b). This characteristic presumably prevented it from affecting the configuration of the displacement deficit anomaly. Nevertheless, the local GNSS network of the Avacha geodynamic testing area recorded a clear response to this event [*Kaftan et al.*, 2025].

The relative proximity of this event to the epicenter of the future 2025 Kamchatka megathrust earthquake (126 km) provides a basis for the hypothetical suggestion of its influence on the early weakening/damage of the source zone of the region's main event. Our assumptions are based on the fact that the focal length of this mega-earthquake is approximately 200–300 km. Our research shows that slow shear deformation waves with propagation velocities of up to 100 km per year can trigger subsequent seismic events [*Kaftan and Melnikov*, 2019; *Kaftan and Tatarinov*, 2022]. A similar trigger mechanism is considered as plausible in the work [*Kishkina and Kocharyan*, 2026] for other events closer in time to the Kamchatka megathrust earthquake.

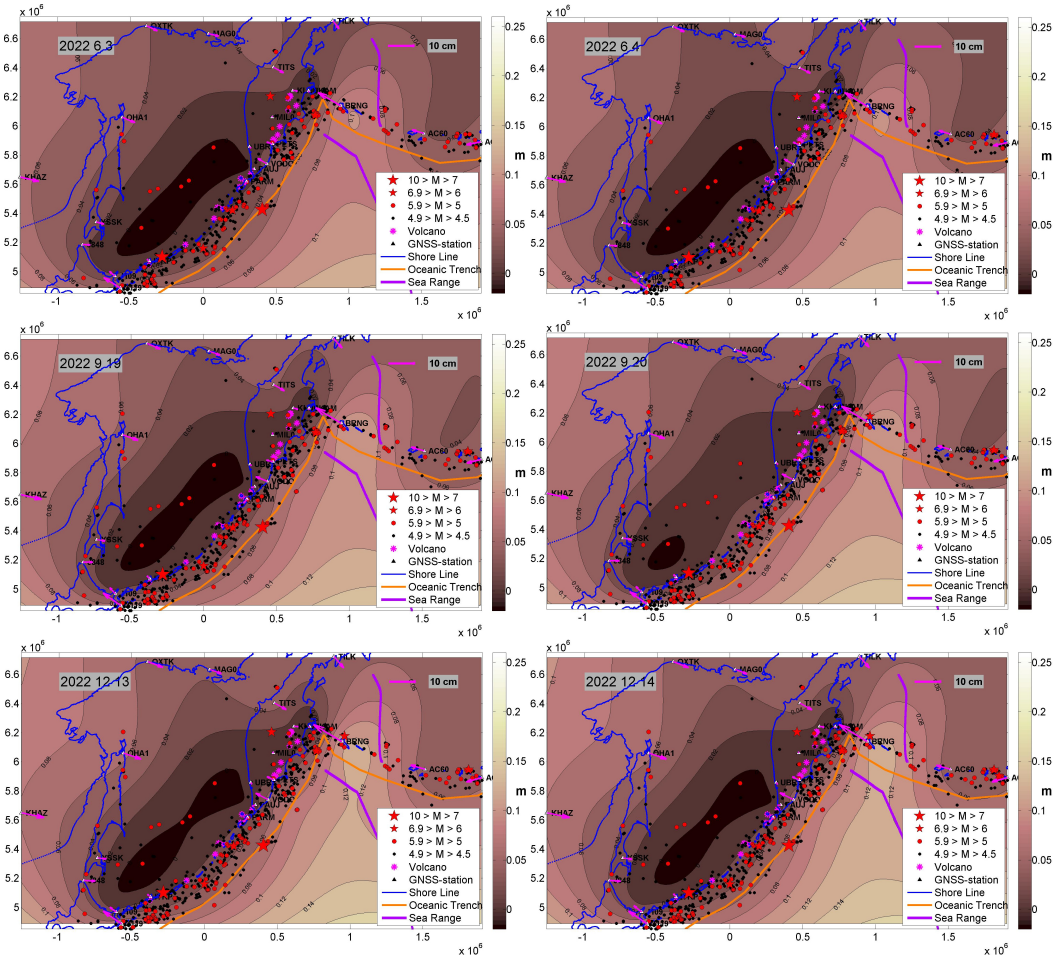

Figure 4. Evolution of the displacement deficit during 2022. a & b – before and after the earthquake of 2022-06-04 (M = 6.3, Depth = 105 km). c & d – before and after the earthquake of 2022-09-20 (M = 6, Depth = 10 km). e & f – before and after the earthquake of 2022-12-14 (M = 6.3, Depth = 73 km). For additional information about the legend, see Figure 1.

The next strong earthquake on 2023-12-28, with M = 6.5, occurred near the Japanese Archipelago islands and did not affect the shape of the displacement deficit anomaly. It is noteworthy that by this time, a significant positive anomaly had formed near Bering Island.

In August 2024, over a two-week period, two strong seismic events with M = 6–7 occurred 50 km north of the future Kamchatka megathrust earthquake's epicenter, at a depth of about 30 km – almost identical to that of the future mainshock. This close proximity to the future main rupture provides grounds to consider these events hypothetically as foreshocks. Notably, the M = 6 event was a natural and expected aftershock of the M = 7 earthquake.

Following the event of 2023-04-03, the displacement deficit in this area decreased from 6 to 10 cm (Figure 5). The peak of rapid displacements increased to 18 cm.

Another strong earthquake with M = 7.4 occurred 9 days before the Kamchatka megathrust earthquake, 47 km to the northeast (Figure 6a, b), continuing to rupture the area of the displacement deficit. The hypocenter of this foreshock was located at a depth of 34 km.

The coseismic effect of the Kamchatka megathrust earthquake is presented in Figure 6c–f. It can be observed that during and after the megathrust earthquake, seismicity propagated southwestward along the deep-sea trench, accompanied by the release of the displacement deficit. The vectors of coseismic displacements demonstrated a direction of movement opposite to their previous interseismic state.

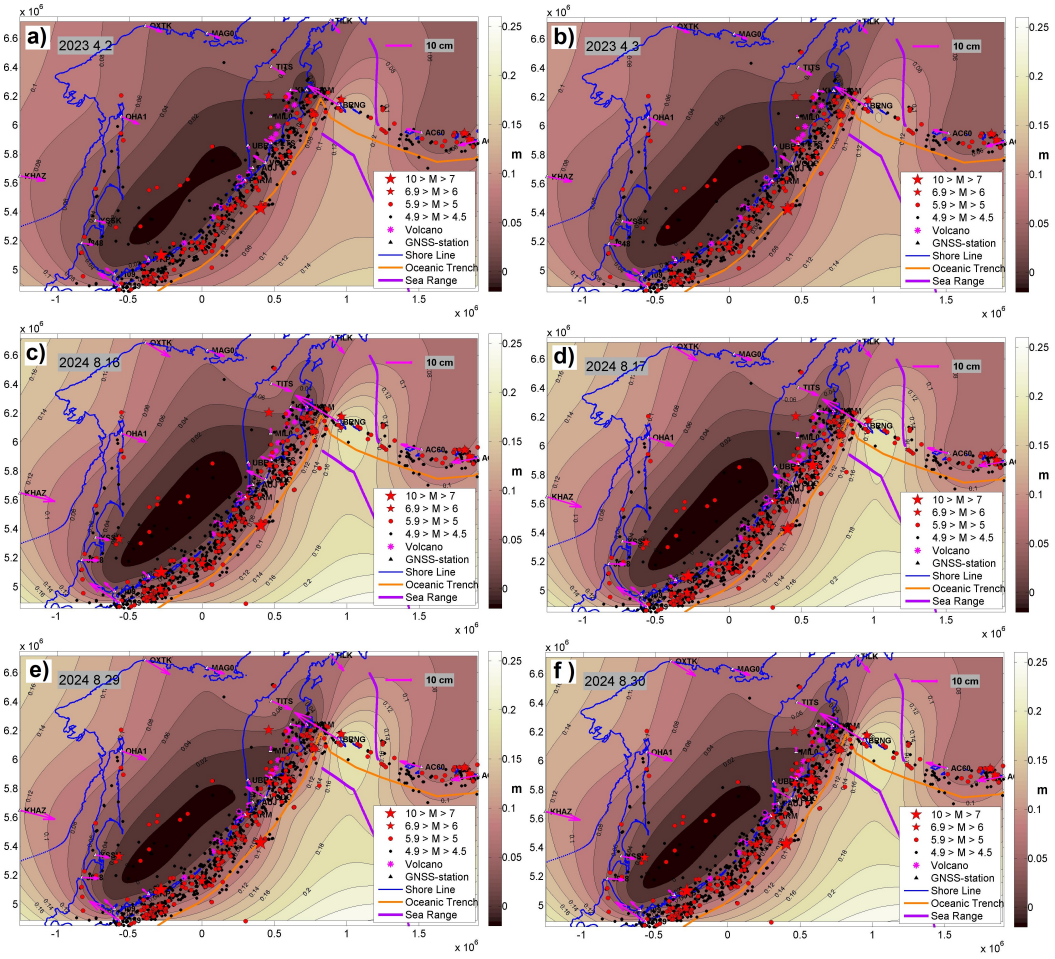

Figure 5. Evolution of the displacement deficit during 2023–2024. a & b – before and after the earthquake of 2023-04-03 (M = 6.5, Depth = 101 km). c & d – before and after the earthquake of 2024-08-17 (M = 7, Depth = 29 km). e & f – before and after the earthquake of 2024-08-30 (M = 6, Depth = 26 km). For additional information about the legend, see Figure 1.

In the internal reference system, the GNSS stations on the eastern coast of Kamchatka shifted southeastward by distances of up to 2 meters. A pattern typical of the elastic rebound model was observed [*Pevnev*, 2021; *Reid*, 1910, 1911; *Savinykh and Pevnev*, 2013]. The rapid displacements fully encompassed the extent of the Kuril–Kamchatka Trench. This is evidenced by the isolines of the light areas in Figure 6d, e, f, the values of which reached decimeters and meters.

A notable observation is that after the release of the elongated zone of horizontal displacement deficit, its extreme (the area of stress accumulation) shifted to the west of the Kamchatka Peninsula coast. We suggest that this area warrants particular attention in terms of anticipating subsequent strong seismic events, which, while less powerful than the Kamchatka earthquake, may be no less hazardous.

5. Analysis of Earth's Crust Movements and Deformations

Based on continuous GNSS observations, the evolution of crustal movements and deformations over more than five years preceding the Kamchatka megathrust earthquake has been investigated.

The nature of spatiotemporal changes in horizontal movements was discussed in the previous section. The analysis of vertical movements (geodetic heights in the ITRF2020 reference frame) did not reveal significant systematic patterns, with the exception of a contrasting coseismic subsidence of Kamchatka's eastern coast by approximately 0.4 m.

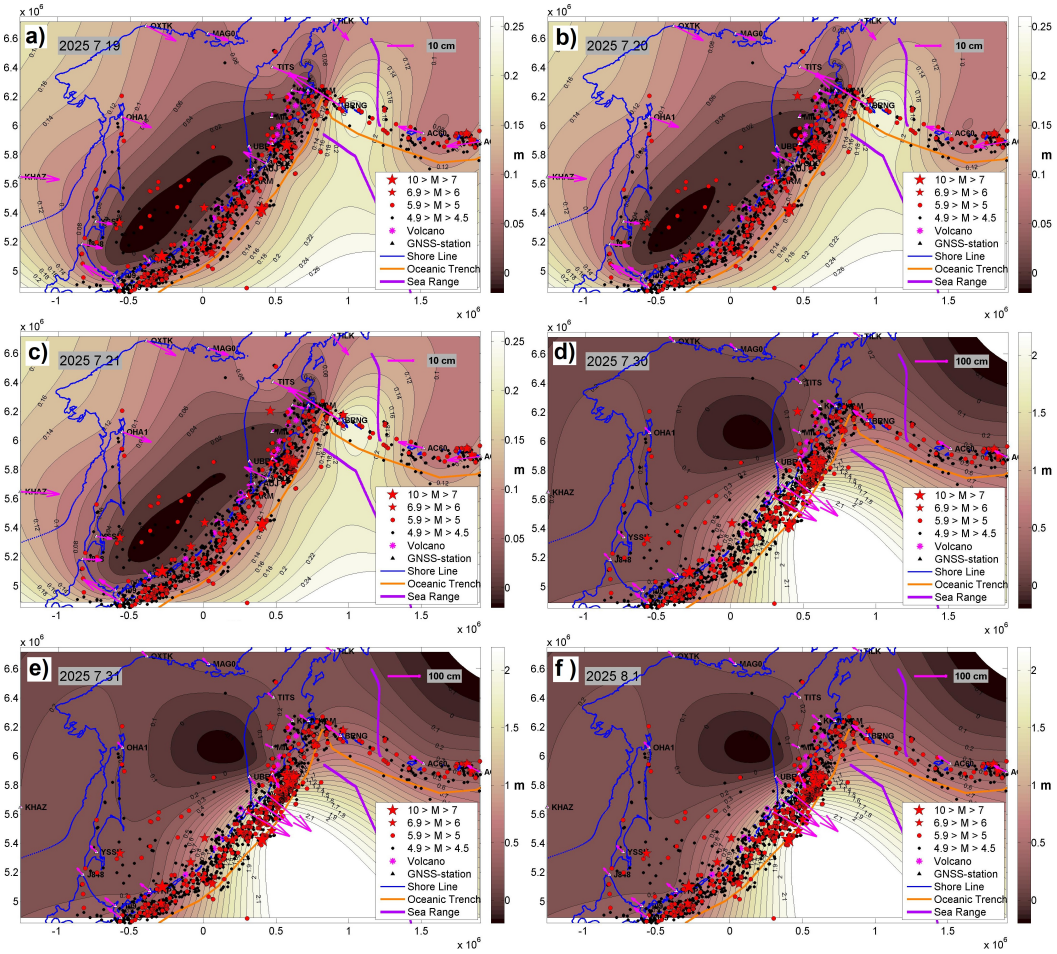

Figure 6. Formation of the displacement deficit during 2025. a & b – before and after the earthquake of 2025-07-20 (M = 7.4, Depth = 58 km). c & d – before and after the earthquake of 2025-07-29 (M = 8.8, Depth = 35 km). e & f – postseismic development of the source following the main event. For additional information about the legend, see Figure 1.

Furthermore, one day prior to the mainshock, minor subsidence of about 2–4 cm accumulated near its epicenter; however, these values are close to the determination errors and do not provide sufficient grounds to claim precursors (Figure 7a, b).

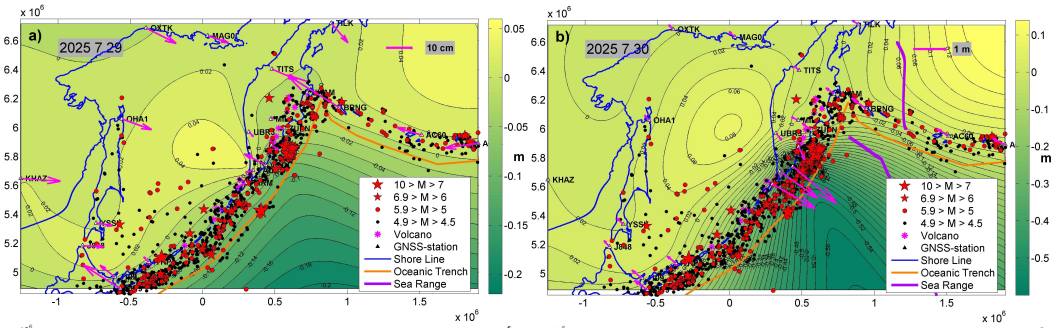

Figure 7. Vertical crustal movements. a) one day before the megathrust earthquake. b) immediately after the megathrust earthquake. For additional information about the legend, see Figure 1.

The dilation deformation evolution [*Dokukin et al.*, 2025c] revealed interesting features (Figure 8). Figure 8 presents key frames of the deformation process. The resulting dilatation distribution pattern indicates the presence of two distinct deformation mechanisms in the region. To discuss this fact, the Kuril–Kamchatka seismic zone is conditionally divided

into two segments. They are separated by the white line segment in Figure 8d, located approximately in the middle of the trench at the transition from tension to compression and at the termination point of the aftershock propagation of the Kamchatka megathrust earthquake. In the southern part, seismicity developed under compression up to 1×10^{-6}, which is consistent with the mechanism of the Pacific Plate pressing against the Okhotsk Block (Figure 8). The northern segment of the trench is subject to extension with a maximum of 5×10^{-7} in the area of the mantle plume head, which creates a local source of pressure and high temperatures beneath the Meiji Guyot [*Gorbatov et al.*, 2001]. Weak compression along the Kamchatka Peninsula suggests the injection of pressure from the mantle flow onto the peninsula's crust, creating an obstacle to the extensional forces.

The anomalous extension grew over more than five years (Figure 8a, b, c). After the megathrust earthquake, the crust of the Kamchatka Peninsula shifted southeastward, forming a zone of compression at the front of the movement and a zone of extension in the rear part (Figure 8d).

The presumed underflow of subcrustal material from the mantle plume, which created extensional strains of up to 5×10^{-6} west of the seismic rupture (Figure 8d), influenced the mechanism of one of the strongest aftershocks ($M = 6.8$, Figure 1). This event exhibited normal faulting, in contrast to the thrust mechanisms of the mainshock and other foreshocks and aftershocks located near the hypocentre (Figure 1). The area of anomalous compression dilatation at the position of the epicenter of the Kamchatka mega-earthquake is consistent with the focal mechanism of the main event and aftershocks (Figure 1).

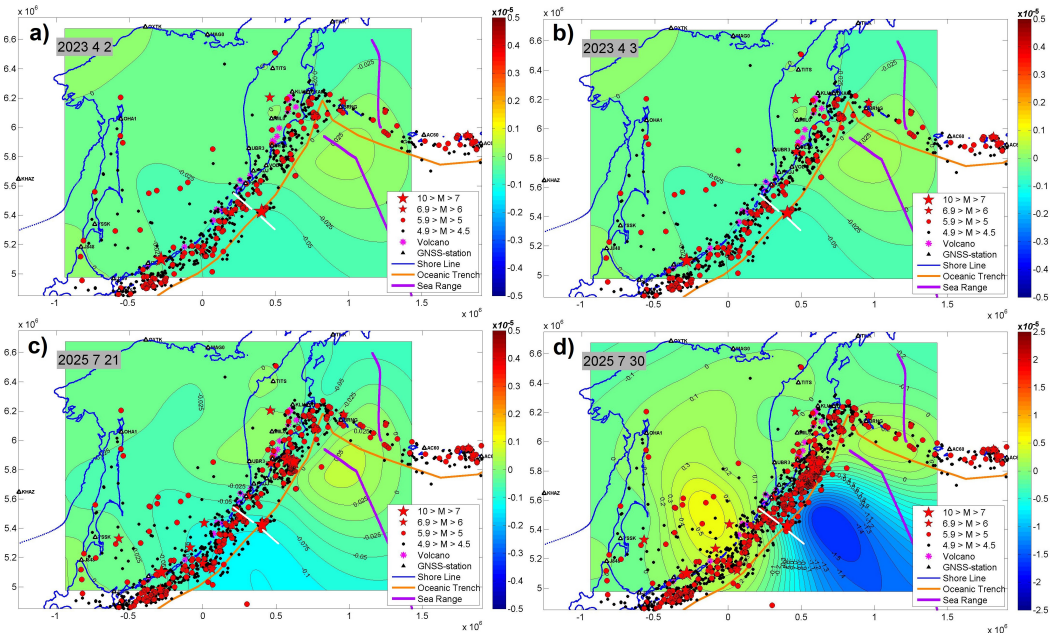

Figure 8. Evolution of dilatational strain from 2020-01-01 to 2025-08-01. a & b – before and after the earthquake in Avacha Gulf on 2023-04-03 ($M = 6.5$, Depth = 101 km). c & d – before and after the earthquake on 2025-07-29 ($M = 8.8$, Depth = 35 km). For additional information about the legend, see Figure 1.

Intense extensional strain of the Earth's surface, associated with the preparation and occurrence of a series of strong earthquakes, was previously identified in the region of the Hikurangi superplume [*Dokukin et al.*, 2023; *Kaftan et al.*, 2024]. The strongest among these was the earthquake near the Kaikōura triple junction (New Zealand) with $M = 7.8$. Extensional strains were also recorded above the submarine base of the Etna volcano edifice [*Kaftan and Rodkin*, 2019] in the waters of the Catania Gulf (Italy). A recent intrusion in the Santorini volcano region showed similar extension [*Dokukin et al.*, 2025a].

Interesting features of the total shear strain evolution in relation to the development of seismicity are demonstrated in a synoptic animation [*Dokukin et al.*, 2025d]. The most significant frames are presented in Figure 9.

It can be observed that during the interseismic period, the total shear strain (Figure 9a, b, c), as well as the dilatational strain, were relatively small, up to 1×10^{-6}. Nevertheless, two extremes formed: one in the southern segment of the Kuril–Kamchatka arc, which is expected due to the motion of the Pacific Plate; and, unexpectedly, in the region of Bering Island.

This area is characterized by the fastest horizontal movements of station BRNG. Research by [*Chekhovich et al.*, 2014] indicates that the tectonics of the Aleutian Trench are governed precisely by strike-slip displacements along its strike. A study of aftershocks from megathrust earthquakes in 1938–2021 revealed a seismic gap in the Bering Island area regarding the expectation of a megathrust earthquake [*Tape and Lomax*, 2022]. This circumstance is also discussed in [*Lobkovsky et al.*, 2014].

In this context, the relatively rapid motion of Bering Island is natural, as rapid movements do not facilitate the accumulation of elastic stresses at a given point.

Two maxima of total shear strain in the northeast and southwest of the region (Figure 9a–c) revealed a seismic quiescence precisely in the area of the future rupture zone of the Kamchatka megathrust earthquake. The merging of these anomalies into a single entity after the mainshock is consistent with the hypothesis of their trigger effect on the future seismic source [*Kaftan and Melnikov*, 2019; *Kaftan and Tatarinov*, 2022].

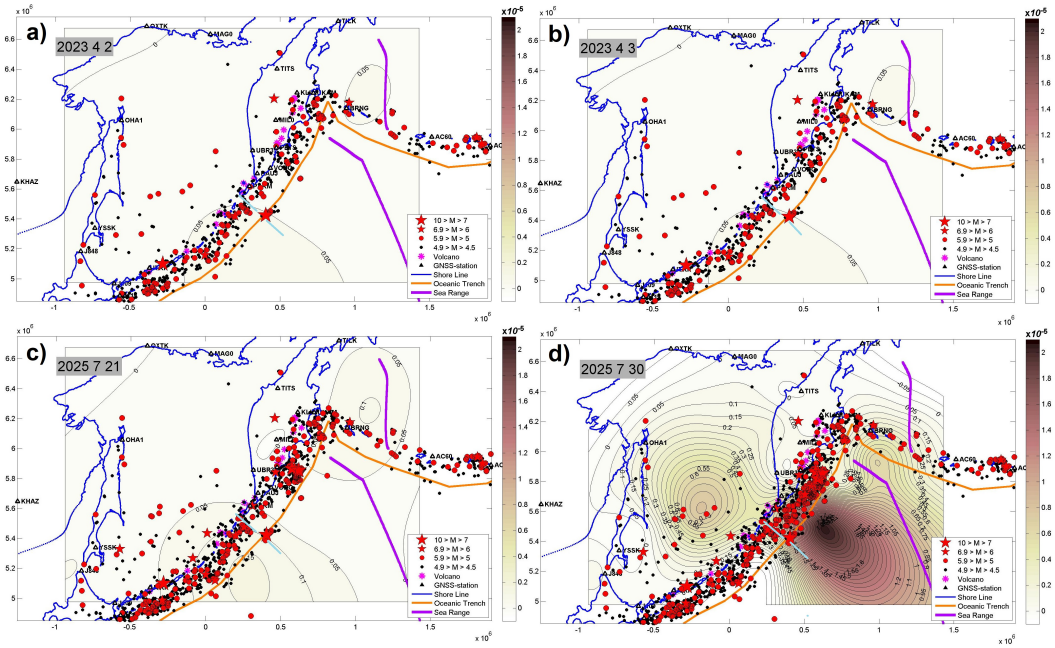

Figure 9. Evolution of total shear strain from 2020-01-01 to 2025-08-01. a & b – before and after the earthquake in Avacha Gulf on 2023-04-03 (M = 6.5, Depth = 101 km). c & d – before and after the earthquake on 2025-07-29 (M = 8.8, Depth = 35 km). For additional information about the legend, see Figure 1.

Figure 9c shows that prior to the Kamchatka megathrust earthquake, the density of epicenters in the southern part of the Kuril–Kamchatka Trench was higher than in the northern part. Here, stress was released more uniformly compared to the northern part, which was awaiting the strongest shock and the swarm of its aftershocks. As a result of the megathrust earthquake, the coseismic total shear strain increased up to 10^{-5}.

6. Discussion and Conclusion

Despite the significant spatial extent and low station density of the GNSS network, the research has shown that such a network provides valuable information on the kinematics of crustal movements and deformations in this region.

The behavior of the displacement deficit demonstrated its systematic concentration along the main seismogenic zone of the Kuril–Kamchatka arc. Over the five years preceding the megathrust earthquake, it clustered into a relatively narrow area, delineating a unified seismic hazard zone. Earthquakes of different magnitudes and depths contributed differently to its release through seismic rupture formation. A more detailed study of this phenomenon will allow for a more reliable assessment of the potential for using surface movements and deformations to evaluate the response of deep-seated processes.

The migration of the seismic hazard zone (the area of minimum displacement deficit) towards the western coast of Kamchatka, according to our assumptions, indicates an increased probability of subsequent strong earthquakes in this area. At the same time, it must be taken into account that the displacement deficit extreme is located in an area without GNSS stations and was obtained through interpolation. This reduces the confidence in our estimates for this region.

As research experience shows, strong earthquakes often occur in the transition zone from fast to slow crustal internal movements. For the eastern margin of this extreme, strong crustal seismicity cannot be ruled out.

The evolution of horizontal dilatational strain revealed two distinct deformation regimes for the segments of the Kuril–Kamchatka arc attributed to the Okhotsk and the supposed Kamchatka microplates. The first is subjected to unidirectional compression from the pressure of the Pacific Plate. In the northern segment of the arc, extensional strain accumulated, coinciding in its location with the "head" of the Meiji Guyot mantle plume.

This phenomenon can be interpreted as the underflow of subcrustal masses beneath the eastern coast of central Kamchatka, creating stress at its contact with the more rigid crust. Bering Island falls within this zone of intense extension and rapid movements. This circumstance may indicate a low probability of the strongest earthquakes in this area.

These results, combined with other studies, demonstrate that the contemporary dynamics of active mantle plumes can be reflected in changes of the Earth's surface.

Regional features of the horizontal total shear deformation revealed the formation and growth of two extremes in the southern segment of the Kuril–Kamchatka arc and in the region of Bering Island. These zones coincide with an area of relatively rapid internal crustal movements. Following the occurrence of the Kamchatka megathrust earthquake, these extremes merged into a single area of coseismic megashear.

Combining this fact with the results of previous studies suggests a bilateral trigger effect of the preseismic total shear deformation extremes on the rupture of the Kamchatka megathrust earthquake source.

The applicability of a sparse regional GNSS network for studying crustal movements and deformations over long time intervals holds promise for obtaining new knowledge on the preparation and rupture nucleation of strong earthquakes.

Acknowledgments. This work was conducted within the framework of the state budgetary funding of the Geophysical Center of the Russian Academy of Sciences (GC RAS), provided by the Ministry of Science and Higher Education of the Russian Federation, and under the State Assignment No. 075-00682-24 ("Interdepartmental Comprehensive Program of Scientific Research in the Kamchatka Peninsula and Adjacent Waters"). The most important supporting information for this article is presented in the video datasets published by the Geophysical Center of the Russian Academy of Sciences (GC RAS) in its Earth Science DataBase (ESDB) repository by *Dokukin et al.* [2025b,c,d]. The study also utilized data obtained from the unique research facility (https://ckp-rf.ru/usu/507436/, http://www.gsras.ru/unu/).

References

Avdeiko G. P., Savelyev D. P., Palueva A. A., et al. Evolution of the Kurile-Kamchatkan volcanic arcs and dynamics of the Kamchatka-Aleutian Junction // Volcanism and Subduction: The Kamchatka Region. — Washington, DC : American Geophysical Union, 2007. — P. 37–55. — https://doi.org/10.1029/172gm04

Blewitt G., Hammond W. C. and Kreemer C. Harnessing the GPS data explosion for interdisciplinary science // Eos. — 2018. — Vol. 99. — https://doi.org/10.1029/2018eo104623

Chebrov D. The Mw=8.8 Kamchatka megathrust earthquake of July 29, 2025 // Bulletin of Kamchatka Regional Association «Educational-Scientific Center». Earth Sciences. — 2025. — 3(67). — P. 113–117. — https://doi.org/10.31431/1816-5524-2025-3-67-113-117 — (In Russian).

Chekhovich V. D., Sheremet O. G. and Kononov M. V. Strike-slip fault system in the Earth's crust of the Bering Sea: A relic of boundary between the Eurasian and North American lithospheric plates // Geotectonics. — 2014. — Vol. 48, no. 4. — P. 255–272. — https://doi.org/10.1134/s0016852114040037

Dokukin P. A., Gök E., Kaftan V. I., et al. Recent crustal movements and deformations in the Aegean sea region in connection with seismicity and volcanism // Natural hazards and disasters: history, forecast, protection. — Saint Petersburg : SPbSUE Publ, 2025a. — P. 155–159. — (In Russian).

Dokukin P. A., Kaftan V. I., Manevich A. I., et al. Evolution of the seismic process and crustal movements (2008-2021) under the influence of the Hikurangi mantle superplume. — Moscow, 2023. — https://doi.org/10.2205/esdb-hikurangi-movement

Dokukin P. A., Kaftan V. I., Titkov N. N., et al. Five-Year Evolution of Regional Seismicity and Deficit of Internal Crustal Displacements According to GNSS Data in Connection with the Kamchatka Megathrust Earthquake of 2025. — Moscow, 2025b. — https://doi.org/10.2205/esdb-kamchatka-2025

Dokukin P. A., Kaftan V. I., Titkov N. N., et al. Five-Year Evolution of Regional Seismicity and Horizontal Dilatation According to GNSS Data in Connection With the Kamchatka Megathrust Earthquake of 2025. — Moscow, 2025c. — https://doi.org/10.2205/esdb-kamchatka-hd-2025

Dokukin P. A., Kaftan V. I., Titkov N. N., et al. Five-Year Evolution of Regional Seismicity and Total Shear Strain to GNSS Data in Connection With the Kamchatka Megathrust Earthquake of 2025. — Moscow, 2025d. — https://doi.org/10.2205/esdb-kamchatka-tss-2025

Fedotov S. A. and Solomatin A. V. Long-Term Earthquake Prediction (LTEP) for the Kuril-Kamchatka island arc, June 2019 to May 2024; Properties of Preceding Seismicity from January 2017 to May 2019. The Development and Practical Application of the LTEP Method // Journal of Volcanology and Seismology. — 2019. — Vol. 13, no. 6. — P. 349–362. — https://doi.org/10.1134/s0742046319060022

Gaedicke C., Baranov B., Seliverstov N., et al. Structure of an active arc-continent collision area: the Aleutian-Kamchatka junction // Tectonophysics. — 2000. — Vol. 325, no. 1/2. — P. 63–85. — https://doi.org/10.1016/S0040-1951(00)00131-1

Gorbatov A., Fukao Y., Widiyantoro S., et al. Seismic evidence for a mantle plume oceanwards of the Kamchatka-Aleutian trench junction // Geophysical Journal International. — 2001. — Vol. 146, no. 2. — P. 282–288. — https://doi.org/10.1046/j.0956-540x.2001.01439.x

Kaftan V. and Melnikov A. Migration of Earth Surface Deformation as a Large Earthquake Trigger // Trigger Effects in Geosystems. — Cham : Springer International Publishing, 2019. — P. 71–78. — https://doi.org/10.1007/978-3-030-31970-0_8

Kaftan V. I., Dokukin P. A., Manevich A. I., et al. Deformation interaction of strong earthquakes of 2010-2016 in the zone of influence of the Hikuranga superplume (New Zealand) according to GPS observations // Geodynamics & Tectonophysics. — 2024. — Vol. 15, no. 1. — P. 0735. — https://doi.org/10.5800/gt-2024-15-1-0735

Kaftan V. I., Mironov I. K., Manevich A. I., et al. Recent Movements and Deformations of the Earth's Crust in the Region of Avacha Volcano (Kamchatka Peninsula) from 2015 to 2023 // Izvestiya, Physics of the Solid Earth. — 2025. — Vol. 61, no. 3. — P. 385–395. — https://doi.org/10.1134/s1069351325700302

Kaftan V. I. and Rodkin M. V. Earth's Surface Deformation on Mount Etna: GPS Measurements, Interpretation, Relationship to the Mode of Volcanism // Journal of Volcanology and Seismology. — 2019. — Vol. 13, no. 1. — P. 7–16. — https://doi.org/10.1134/s0742046319010032

Kaftan V. I. and Tatarinov V. N. Registration of Slow Deformation Waves According to GNSS Observations // Doklady Earth Sciences. — 2022. — Vol. 505, no. 1. — P. 489–495. — https://doi.org/10.1134/s1028334x22070091

Kishkina S. B. and Kocharyan G. G. Possible Triggers of the Great Kamchatka earthquake 29.07.2025, Mw 8.8 // Dynamic Processes in Geospheres. — 2026. — Vol. 17, no. 4. — P. 1–11. — https://doi.org/10.26006/29490995_2025_17_4_1 — (In Russian).

Kocharyan G. G., Kishkina S. B., Novikov V. A., et al. Slow slip events: parameters, conditions of occurrence, and future research prospects // Geodynamics & Tectonophysics. — 2014. — Vol. 5, no. 4. — P. 863–891. — https://doi.org/10.5800/gt-2014-5-4-0160 — (In Russian).

Lobkovsky L. I., Baranov B. V., Dozorova K. A., et al. The Komandor seismic gap: Earthquake prediction and tsunami computation // Oceanology. — 2014. — Vol. 54, no. 4. — P. 519–531. — https://doi.org/10.1134/s0001437014030072

Materna K., Murray J., Pollitz F., et al. Slip Deficit Rates on Southern Cascadia Faults Resolved with Viscoelastic Earthquake Cycle Modeling of Geodetic Deformation // Bulletin of the Seismological Society of America. — 2023. — Vol. 113, no. 6. — P. 2505–2518. — https://doi.org/10.1785/0120230007

Pevnev A. K. Substantiation of the main concepts for the deformation model of the crustal earthquake source preparation // Geology and Geophysics of Russian South. — 2021. — Vol. 11, no. 1. — P. 104–120. — https://doi.org/10.46698/vnc.2021.53.34.009

Pinegina T. K., Ozerov A. Y., Tsvetkov V. A., et al. Tsunami from the Mw 8.8 Kamchatka Earthquake of 29 July 2025 on the East Coast of Kamchatka and the North Kuril Islands // Pure and Applied Geophysics. — 2026. — Vol. 183, no. 1. — P. 1–25. — https://doi.org/10.1007/s00024-025-03873-1

Plata-Martinez R., Iinuma T., Tomita F., et al. Revisiting Slip Deficit Rates and Its Insights Into Large and Slow Earthquakes at the Nankai Subduction Zone // Journal of Geophysical Research: Solid Earth. — 2024. — Vol. 129, no. 12. — https://doi.org/10.1029/2023jb027942

Pushcharovsky Y. M. First-order linear tectonovolcanic ridges in oceans // Geotectonics. — 2011. — Vol. 45, no. 2. — P. 101–112. — https://doi.org/10.1134/s0016852111020051

Reid H. F. Permanent displacements of the ground // The California Earthquake of April 18, 1906. Volume II. The mechanics of the earthquake. — Carnegie Institution of Washington, 1910. — P. 16–28.

Reid H. F. The elastic-rebound theory of earthquakes // Bulletin of the department of Geology. University of California Publication. — 1911. — Vol. 6, no. 19. — P. 413–444.

Savinykh V. P. and Pevnev A. K. Using space methods to predict earthquakes // Izvestia Vuzov. Geodesy and Aerophotosurveying. — 2013. — No. 2. — P. 24–30. — (In Russian).

Steblov G. M., Vasilenko N. F., Prytkov A. S., et al. Dynamics of the Kuril-Kamchatka subduction zone from GPS data // Izvestiya, Physics of the Solid Earth. — 2010. — Vol. 46, no. 5. — P. 440–445. — https://doi.org/10.1134/s1069351310050095

Tape C. and Lomax A. Aftershock Regions of Aleutian-Alaska Megathrust Earthquakes, 1938-2021 // Journal of Geophysical Research: Solid Earth. — 2022. — Vol. 127, no. 7. — https://doi.org/10.1029/2022jb024336

Wu J. C., Tang H. W., Chen Y. Q., et al. The current strain distribution in the North China Basin of eastern China by least-squares collocation // Journal of Geodynamics. — 2006. — Vol. 41, no. 5. — P. 462–470. — https://doi.org/10.1016/j.jog.2006.01.003